POST-EPS WINDSCATTEROMETER CONCEPT TRADE-OFFS AND WIND RETRIEVAL PERFORMANCE ASSESSMENT

C.C. Lin[1], M. Betto[1], M. Belmonte Rivas[2], A. Stoffelen[3], J. de Kloe[3]

[1] ESA-ESTEC, Keplerlaan 1, 2200 AG Noordwijk, The Netherlands
Tel.: +31-71-5655813; Fax.: +31-715655301; E-mail: Chung-Chi.Lin@esa.int
[2] Dept. of Aerospace Eng. Sciences, Univ. of Colorado, UCB 429, Boulder, CO 80309-0429
[3] KNMI, Wilhelminalaan 10, 3732 GK De Bilt, The Netherlands

Abstract

The Post-EPS (or EPS-Second Generation) mission will be deployed in the 2018 – 2020 timeframe in order to ensure continuity of the EUMETSAT Polar System (EPS) observation missions, currently realised with the *MetOp* satellite series, to support **operational meteorology**, in particular for the numerical weather predictions (NWP), **climate monitoring** and to develop new **environmental services**. The Scatterometer (SCA) is one of the high priority payload instruments to provide vector surface wind observations over ocean, which constitute an important input to the NWP as well as valuable information for tracking of extreme weather events. The Post-EPS SCA shall offer observations with higher spatial resolution than those provided by ASCAT on board *MetOp*. Furthermore, addition of HH polarization is considered as an option.

Phase 0 industrial studies, addressing the complete system design, have taken place from 2008 to 2009. Two study teams, constituted respectively by Astrium SAS and Thales Alenia Space Italy, have performed comprehensive analyses of the system requirements, trade-offs of various concepts and preliminary design of the selected concepts, which included both the single and dual satellite configurations. Two distinct SCA concepts were elaborated during Phase 0: (1) Fixed fan-beam concept with 6 fixed antennas; (2) Rotating fan-beam concept with a single rotating antenna. The fixed fan-beam concept was selected as baseline after a final trade-off.

For supporting the above instrument concept elaboration by the industrial study teams during Phase 0, KNMI has developed retrieval algorithms tailored to the two concepts, derived from the ASCAT operational algorithms, and specific metrics to characterize the associated retrieval performance. The metrics used for the present performance assessment were: (a) Wind vector RMS error; (b) Ambiguity susceptibility, and; (c) Wind biases. The end-to-end performance evaluation makes use of an ensemble of wind-fields as input having the mean climatological distribution, generates the output wind-fields which account for the measurement system imperfections and geophysical noise, and compute the performance metrics for comparisons.

This paper describes the two SCA concepts as derived in Phase 0 studies by the industrial study teams and summarises the technical trade-offs carried out. The performance metrics are described and applied to the two concepts in order to compare their respective merits. It is shown that both concepts are able to meet the observation requirements of Post-EPS.

Keywords: EUMETSAT Polar System (EPS), Post-EPS, Windscatterometer, ocean wind, wind retrieval

1. Introduction

The EUMETSAT Polar System (EPS) is a meteorological data acquisition system based on the *MetOp* series of low-Earth orbiting satellites. A successor programme, Post-EPS (or EPS Second Generation) will replace EPS in the 2018–2020 timeframe [1][2]. The Scatterometer (SCA) is one of the high priority payload instruments to provide vector surface wind observations over ocean, which constitute an important input to the NWP as well as valuable information for tracking of extreme weather events. The secondary products derived from the scatterometer data are:

- Land surface soil moisture
- Leaf area index
- Snow water equivalent
- Snow cover
- Sea-ice type
- Sea Ice extent.

The Post-EPS SCA shall offer observations with higher spatial resolution and radiometric stability than those provided by ASCAT on board *MetOp*. Furthermore, addition of HH polarization is considered as an option.

Phase 0 industrial studies, contracted respectively to Astrium SAS and Thales Alenia Space Italy, addressing the complete system design, have taken place from 2008 to 2009. Following the recommendations made at the end of Phase 0, EUMETSAT council agreed in June 2010 that a two-satellite configuration will be assumed for phase A/B1 studies. In this scenario, the mission will be implemented with a sequence of identical pairs of EPS-SG satellites (A1, B1, A2, B2…), with payload instruments distributed appropriately on the two satellites (A and B), taking into account of constraints on the co-registration requirements among some of them.

Two distinct SCA concepts were elaborated during Phase 0: (1) Fixed fan-beam concept with 6 fixed antennas; (2) Rotating fan-beam concept with a single rotating antenna [3]. The fixed fan-beam concept was selected as baseline after a final trade-off.

For supporting the above instrument concept elaboration by the industrial study teams during Phase 0, KNMI has developed retrieval algorithms tailored to the two concepts, derived from the ASCAT operational algorithms, and specific metrics to characterize the associated wind retrieval performance.

2. Scatterometry (SCA) Technical Requirements

The SCA payload is a real-aperture, pulsed imaging radar with six, fixed fan beam-antennas in the baseline configuration at the conclusion of Phase 0. In this configuration, the principal elevation planes of the SCA antenna beams are oriented at 45° (Fore-left), 90° (Mid-left), 135° (Aft-left), 225° (Aft-right), 270° (Mid-right) and 315° (Fore-right) with respect to the flight direction, similar to the *MetOp*'s ASCAT as shown in Fig. 1. Each of the SCA beams shall acquire a continuous image of the normalised (per-unit-surface) radar backscatter coefficient of the ocean surface, called σ^0 over a swath. Both sides of the sub-satellite track are imaged each with three azimuth views, with an unavoidable observation gap below the satellite. A large number of independent looks are summed in range and azimuth (multi-looking) for each azimuth view in order to achieve the specified radiometric resolution of the σ^0 estimate on each measurement pixel. The three σ^0 measurements (σ^0-triplet) are uniquely related to the 10 m vector wind through the Geophysical Model Function (GMF) [4]. The

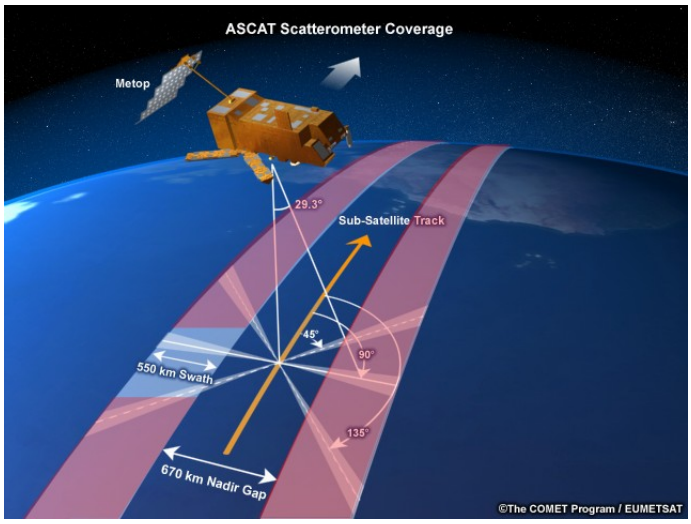

wind inversion is based on a search for minimum distances between the σ^0-triplet and backscatter model solutions lying on the GMF surface, taking into account of the instrument noise estimate and geophysical noise [5]. Due to those noises associated with the measurements, multiple solutions are usually found (wind ambiguities), which are subsequently filtered out using the background wind information (ambiguity removal).

Fig. 1: ASCAT measurement geometry as basis for SCA baseline

As compared to ASCAT, SCA shall have a smaller nadir gap by reducing the minimum incidence angle from 25° (ASCAT) to 20°. The main technical requirements of SCA are:

Frequency:	5.3 GHz
Polarisation:	VV as baseline (+ HH on a reduced set of beams as option)
Number of azimuth views:	≥ 3, ideally separated by 45° each
Incidence angle:	≥ 20°
Dynamic range:	4 – 25 m/s (≤ 40 m/s in case of HH implementation)
Horizontal resolution:	25 km × 25 km
Horizontal sampling:	12.5 km × 12.5 km
Radiometric resolution:	≤ 3 % for $\theta_i \leq 25°$ at 4 m/s cross-wind
	≤ $(0.175 \times \theta_i - 1.375)$ % for $\theta_i > 25°$ at 4 m/s cross-wind
Radiometric stability:	≤ 0.1 dB
Absolute radiometric bias:	≤ 0.35 dB peak-to-peak per beam
Coverage:	≥ 97 % in 48 hours

The major improvements to be brought by SCA with respect to ASCAT are the spatial resolution of 25 km × 25 km and the radiometric stability of ≤ 0.1 dB.

3. Instrument Concept Trade-offs

Three distinct instrument concepts were considered at the start of Phase 0:

(1) Fixed fan-beam scatterometer (e.g. ASCAT, ERS-SCAT, NSCAT);

(2) Rotating fan-beam scatterometer (e.g. RFSCAT [3]);

(3) Rotating pencil-beam scatterometer (e.g. SeaWinds [6]).

Fixed fan-beam concept:

The fixed fan-beam concept has a strong heritage from ASCAT with excellent radiometric performance and good coverage. The observation geometry (Fig. 1) is optimum over the whole swath in terms of azimuth diversity with three views (45°, 90° and 135° w.r.t. syb-satellite track) which maximizes the wind directional sensitivity. This observation geometry

results in a nearly uniform wind retrieval performance over the swath when the radiometric performance is appropriately scaled with incidence angle (see the radiometric resolution requirement in Section 2). One major drawback of the concept is the unavoidable nadir observation gap, which is as large as 670 km for ASCAT. This can be reduced to 520 km when the minimum incidence angle is reduced to 20° below which the wind directional sensitivity is seriously degraded in the GMF.

With the beams fixed in constant azimuth angles, a large number of azimuth looks are generated, which is proportional to the radar pulse repetition frequency (PRF). The net result is a low number of range looks needed to meet the radiometric resolution requirement, leading to a lower bandwidth, hence a relatively low RF-power. The concept nevertheless requires six antennas in order to cover both sides of the sub-satellite track, together with a beam-switching matrix. A subset of the antennas has to be stowed for launch and deployed in orbit.

The antenna length will have to be increased with respect to those of ASCAT in order to meet the horizontal resolution requirement (see Section 4). Due also to the increased system bandwidth in order to achieve the required number of looks within the 25 km × 25 km resolution cell, a higher RF-power is needed with respect to that of ASCAT. Two possible pulsed concepts were considered: (1) a long modulated pulse, low PRF concept (ASCAT heritage); (2) a short un-modulated pulse, high PRF concept (ERS-SCAT heritage). Both concepts are feasible, resulting in a similar DC-power budget.

Rotating fan-beam concept:

The rotating fan-beam scatterometer (Fig. 2) makes use of a single fan-beam antenna rotated around a nadir axis with a speed of approximately 2~3 RPM. The initial concept was studied and performance assessed by Lin et al. [3][7][8]. The slow rotation of the antenna, combined with the range-gating of the radar echo result in multiple azimuth acquisitions of measurement cells during an over-flight. As opposed to the fixed fan-beam concept, the number of azimuth views varies across the swath and is a function of the rotation speed. The azimuth diversity degrades around the nadir and the swath-edges due to the measurement geometry. Thus despite the continuous coverage by the antenna beam, the wind retrieval performance degrades in those regions due to ambiguities in the retrieved wind.

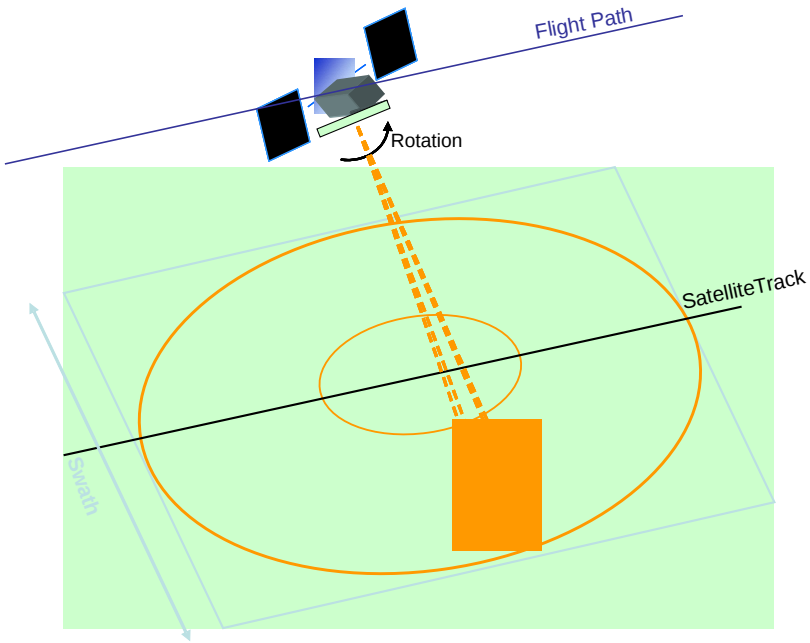

Fig. 2: Rotating fan-beam scatterometer (RFSCAT)

Nevertheless, a compliant performance can be achieved between the stand-off distances from the sub-satellite track of 100 and 800 km (see Section 6) for scan speed of larger than 2 RPM,

leaving a nadir gap of 200 km as compared to 520 km of the fixed fan-beam concept. The necessary antenna dimension, for achieving the required spatial resolution, is similar to that of the Mid-antenna of the fixed fan-beam concept (≅ 2.7 to 2.9 m). A rotating RF-joint is needed for the connection between the radar frontend and the antenna.

The slow rotation of the antenna translates to a faster scan of the antenna footprint over the ocean surface as compared to that of the fixed fan-beam concept. Thus, the number of azimuth looks is correspondingly reduced, which needs to be compensated by increasing the number of range looks. Consequently, the range resolution has to be increased, i.e. the system bandwidth proportionally to the number of range looks. For maintaining the minimum signal-to-noise ratio (SNR) in the vicinity of 0 dB [9], the transmit power needs to be increased. The net result is an increase of the radar DC-power proportionally to the antenna scan speed. As will be seen in Section 5, a minimum scan speed of 2 RPM would be required for meeting the desired wind quality.

The design of the instrument is in principle simpler than that of the fixed fan-beam concept: it requires a single rotating antenna under the nadir face of the spacecraft, i.e. no switching matrix (replaced by an RF rotary joint) and no deployment in orbit. Nevertheless, the life expectancy and RF stability of the rotary joint may be an issue (although the total number of rotation is an order of magnitude lower than those of microwave imaging radiometers). Avoiding field-of-view conflicts with other instruments may be difficult in the case of multi-payload mission. The overall DC-power requirement and data rate are higher than those of the fixed fan-beam concept, but the mass budget is lower due to the reduction of the number of antennas (six to one).

Rotating pencil-beam concept:

The rotating pencil-beam concept has heritages from the SeaWinds scatterometers [6]. A pair of pencil-beams, respectively pointed at two different incidence angles, is rotated around the nadir axis (conical scan) as shown in Fig. 3. Within the swath region sustained by the inner beam (pink on Fig. 3), 4 azimuth views are acquired on each measurement cell, two forward and two backward, with azimuth angles dependent on the swath position. For measurement cells lying between the inner and outer beams, only two azimuth views are obtained. Unambiguous wind retrieval is possible for those cells having four distinct azimuth views, with performance degrading around the sub-satellite track and edges of the inner beam due to the non-ideal measurement geometries.

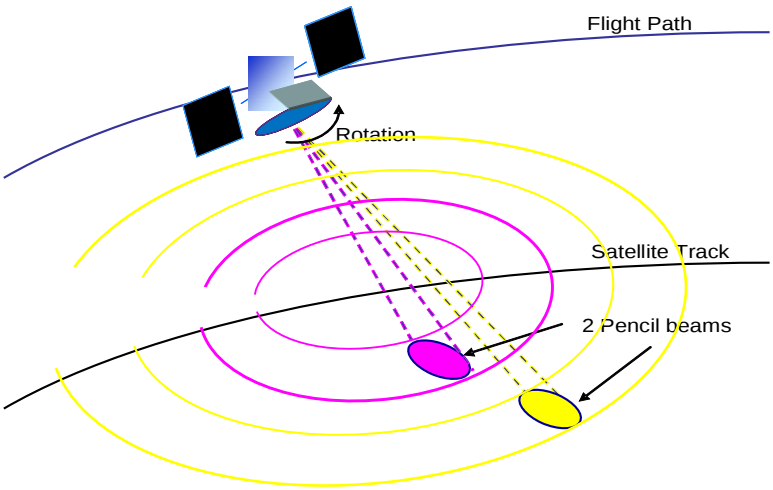

Fig. 3: Rotating pencil-beam scatterometer

In the case of real-aperture concept such as SeaWinds, the high rotation rate of the antenna (e.g. 18 RPM), necessary for achieving gap-less coverage from one scan rotation to the next,

results in a low number of azimuth looks. Thus, a high number of range looks is required in order to meet the required radiometric resolution, i.e. a high system bandwidth, resulting in some significant transmit power requirement for meeting the optimum SNR. Therefore, it is generally difficult for this concept to meet the required radiometric resolution as examplified by the SeaWinds scatterometer with its noisier data in comparison to those of ASCAT.

Synthetic Aperture Radar (SAR) processing, combined with a high PRF, could substantially increase the number of azimuth looks. Such a concept was studied by NASA/JPL for the next generation SeaWinds scatterometer. The increased number of azimuth looks, when combined with the range looks, would allow for meeting the radiometric resolution requirement. Nevertheless, the high PRF and the necessary system bandwidth would result in high data rate and SAR processing of the raw data. The SAR processing could be complex due to the constantly changing Doppler-centroid of the radar echo as function of the beam position.

Finally, the major drawback of the rotating pencil-beam concept is the necessity of a large rotating antenna aperture. At C-band, the required aperture would have a diameter of 3 m (as compared to 1 m at Ku-band), rotating at a scan rate of approximately 18 RPM. Accommodation of a large aperture rotating antenna would cause considerable difficulties at the satellite level such as dynamic balancing of the rotating mass and provision of a free field-of-view around the antenna. In comparison to the rotating fan-beam concept, the life expectancy and RF stability of the rotating joint are aggravated by the much higher scan rate. For those reasons, the rotating pencil-beam concept was discarded very early in the Phase 0 trade-offs.

4. Baseline Instrument Design

The fixed fan-beam concept with six antennas has been selected as baseline at the end of Phase A. The observation swaths extend from 260 km to 900 km stand-off distances on both sides of the sub-satellite track. The baseline antenna configuration (VV polarization only) is shown in Fig 4, which consists of 3 pairs of planar arrays arranged in an inversed Y-configuration, to be accommodated on the nadir face of the spacecraft. Fore- and Aft-antenna assemblies shall be stowed for launch and deployed in orbit. The three antenna assemblies can be configured differently if necessary for accommodation reasons, provided that the respective orientation in azimuth is maintained.

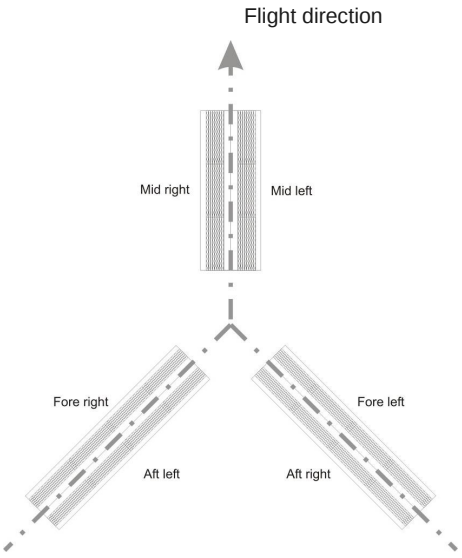

The antennas consist of slotted waveguide arrays, made of metallised carbon-fibre reinforced plastic (CFRP) in order to meet the stringent radiometric stability requirement. They are connected through waveguides to the beam-switching matrix. For the Fore-/Aft-antenna assemblies, rotating RF-joints are required for enabling deployment. Each of the antenna assembles is mounted on a CFRP support structure for ensuring a very high pointing stability.

Fig. 4: SCA antenna configuration: Mid-antenna assembly is 2.7 to 2.9 m long; Fore- and Aft-antenna assemblies are 3.5 m long.

The instrument block diagram is depicted in Fig. 5. The baseband radar pulse is stored in the digital memory read-out and followed by the digital-to-analogue converter (DAC). The

analogue pulse is then up-converted to the carrier frequency by a quadrature mixer. The trade-off between the non-modulated and modulated transmit pulse is still on-going, and this will have impacts on the radar PRF and peak power necessary from the high power amplifier (HPA). The HPA consists of a traveling wave tube (TWA) driven by a high voltage electronics power conditioner (EPC). The HPA feeds the six antennas sequentially through the beam-switching matrix.

The receive signal is amplified by the low noise amplifier (LNA) and down-converted to the in-phase (I) and quadrature phase (Q) baseband signals. The digitized I and Q baseband signals could be detected and multi-looked on board (incoherent summation of the detected echo-profiles). In the case of modulated pulse concept, the I and Q signals are first pulse-compressed before detection. Alternatively, the digitized I and Q signals could be down-linked and further processed on ground. The later option would substantially increase the data amount to be down-linked with corresponding system impacts.

The internal calibration loops measure the transmit pulses at the input and output of the HPA, as well as at the input of the LNA. Those measurements enable gain characterization of the transmit- and receive-chains, as well as losses of the components in the radar frontend. The necessity of measuring the pulses at the input ports of the antennas is a subject of further analysis in relation to meeting the radiometric stability requirement.

Table 1 summarises the major design parameters. Instrument mass and power estimates at the end of Phase 0 are respectively 360 kg and 720 W for the baseline (VV) concept. Implementation of the HH-polarisation on a subset of beams, in addition to the VV-polarisation on all beams, is a subject of further trade-offs. HH-polarisation is desirable for extending the upper dynamic range of the wind measurements ($\leq$ 40 m/s) and for improving the quality of soil moisture product over land.

Fig. 5: SCA instrument block diagram

Table 1: SCA design parameters and overall budgets

5. End-to-End Performance Assessment Methodology

The scatterometer performance assessment methodology rests on the output wind statistics produced by an end-to-end scatterometer wind retrieval simulator, which is schematically shown in Fig. 6. The scatterometer wind retrieval simulator converts an input wind vector ($\mathbf{v}_{IN}$) extracted from a world wind climatology into a vector of error/noise-free backscatter coefficient measurements using the GMF sampled at observation angles specified by the scatterometer observation geometry. Measurement noise is then added to these backscatter coefficients according to the estimated system (instrumental + geophysical) noise levels, and injected to the wind retrieval core of the simulator to generate an output wind vector ($\mathbf{v}_{OUT}$). After a large number of wind inversions (or Monte-Carlo runs), the output wind solutions are collected and binned into output wind distribution functions $P_{obs}(\mathbf{v}_{OUT}|\mathbf{v}_{IN})$, which describe the statistical distribution of wind outputs for a particular wind input and allow the characterization of the retrieval error incurred by a particular scatterometer concept via mean statistics such as the wind vector root-mean-square (RMS) error, the wind vector bias or the presence of multiple ambiguous solutions. The climatologically averaged performance is then finally computed by repeating the above procedure over the wind climatology (see Fig. 7

below). The following sections describe in detail how these processes are implemented.

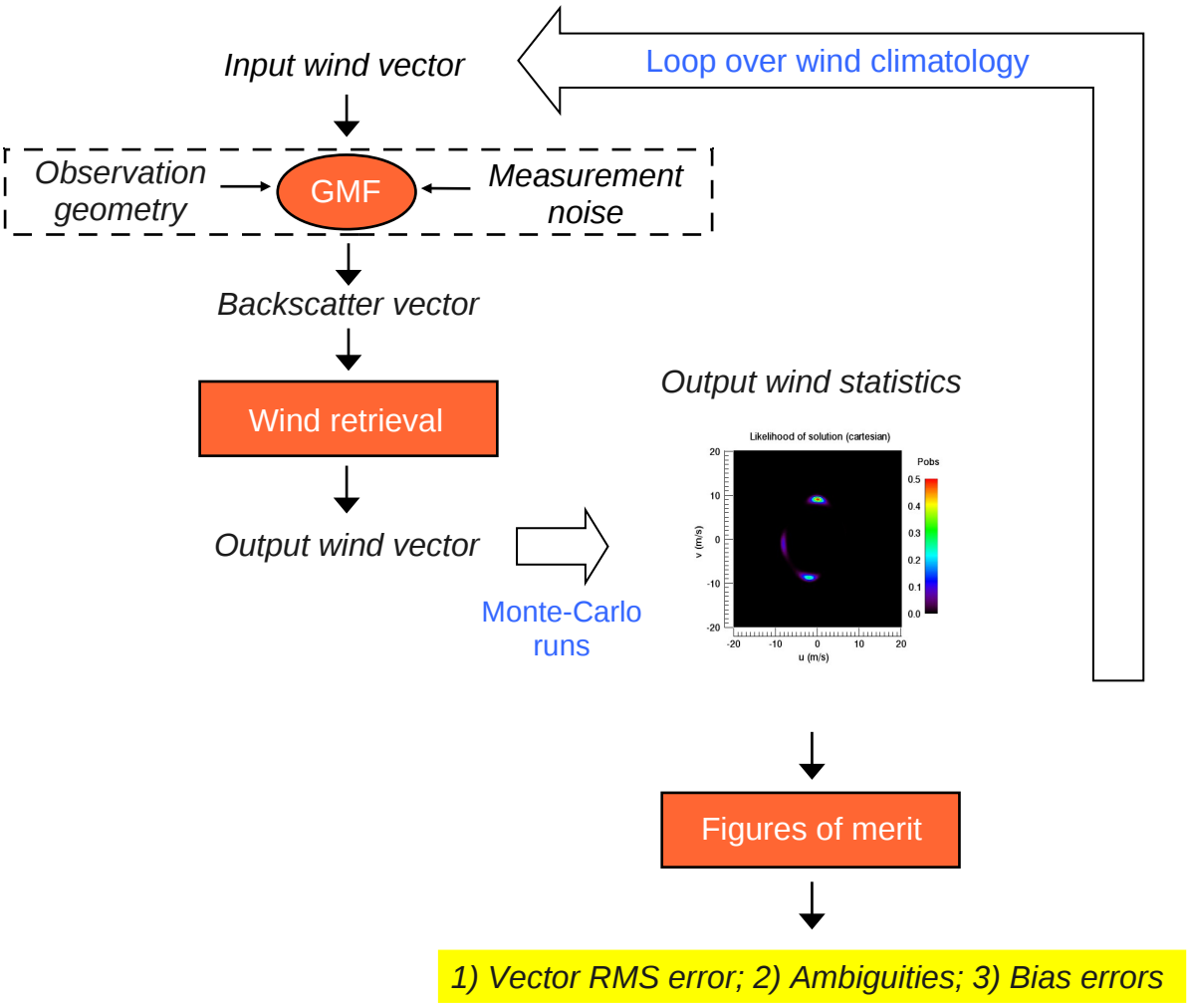

$$P_{obs}\left(\right.$$

Fig. 6: End-to-end scatterometer performance assessment methodology

Input wind:

The retrieval of ocean wind vectors in scatterometry is a non-linear problem and the error characteristics of the wind output depend on the wind input state. To eliminate this undesirable dependence on initial conditions, the scatterometer error characteristics are to be averaged over a world climatology of wind inputs characterized by a Weibull distribution in wind speeds [10], as given by Eq. (1), with a maximum around 8 m/s (see Fig. 7) and a uniform distribution in wind direction.

$$f(v) = \frac{p2}{p1}\left(\frac{v}{p1}\right)^{p2-1} e^{-\left(\frac{v}{p1}\right)^{p2}} \quad (1)$$

where $p1$ = 10 m/s and $p2$ = 2.2 m/s.

The input wind speeds are discretized from 3 to 16 m/s using steps of 1 m/s, covering about 90 % of ocean wind states. The input wind directions are discretized from 0 to 360 degrees using steps of 10 degrees.

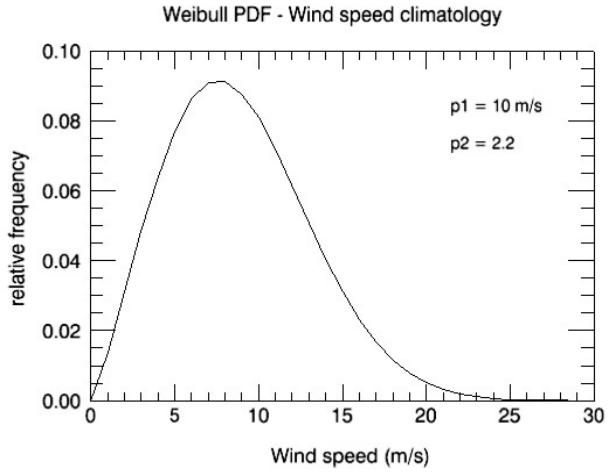

Fig. 7: Wind speed climatology (Weibull PDF [10])

Geophysical Model Function (GMF):

The GMF is an empirically derived function that relates backscatter measurements to surface wind vectors and viewing geometries in the form of σ^0 = GMF (incidence angle, azimuth angle, wind vector). For C-band VV simulations, we use the CMOD5 model (see Fig. 8) for ocean backscatter [4], which is valid for incidence angles ranging from 18 to 58 degrees. For Ku-band VV and HH simulations, we use the NSCAT backscatter numerical tables (see Fig. 9) [11].

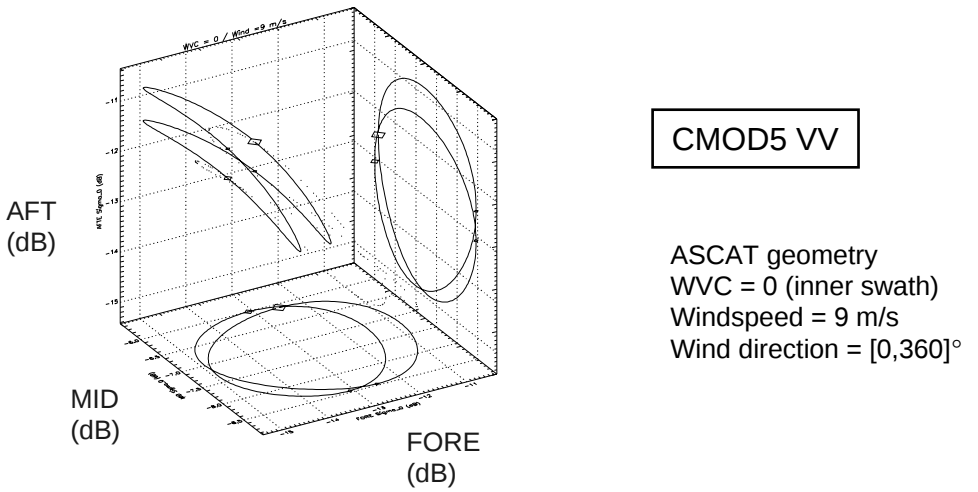

Fig. 8: CMOD5: C-band GMF in ASCAT measurement space (3 views)

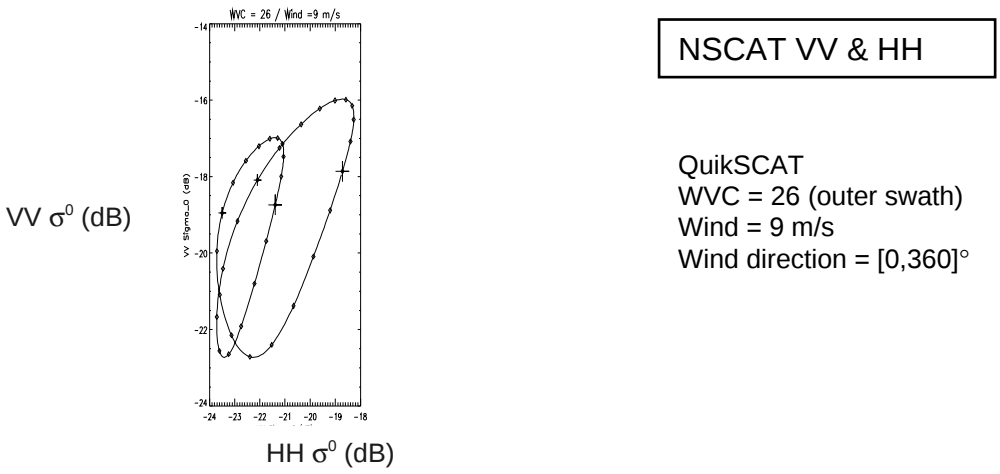

Fig. 9: NSCAT: Ku-band GMF in QuikScat measurement space (4 views)

Observation geometry:

The correct determination of the ocean wind vector signature requires that every wind vector cell (WVC) on the surface be visited by a number of views from a diversity of observation angles. The observation geometry refers to the sequence of view (incidence and azimuth) angles at which the scatterometer beams intersect the surface, which is in general a function of the across-track distance of the WVC node, and of the beam rotation speed and timing for a rotating system. The observation geometry is calculated for every node on the swath using a simplified orbital model together with specific scatterometer instrument model parameters and stored as Pseudo-Level 1b products as shown in Fig. 10.

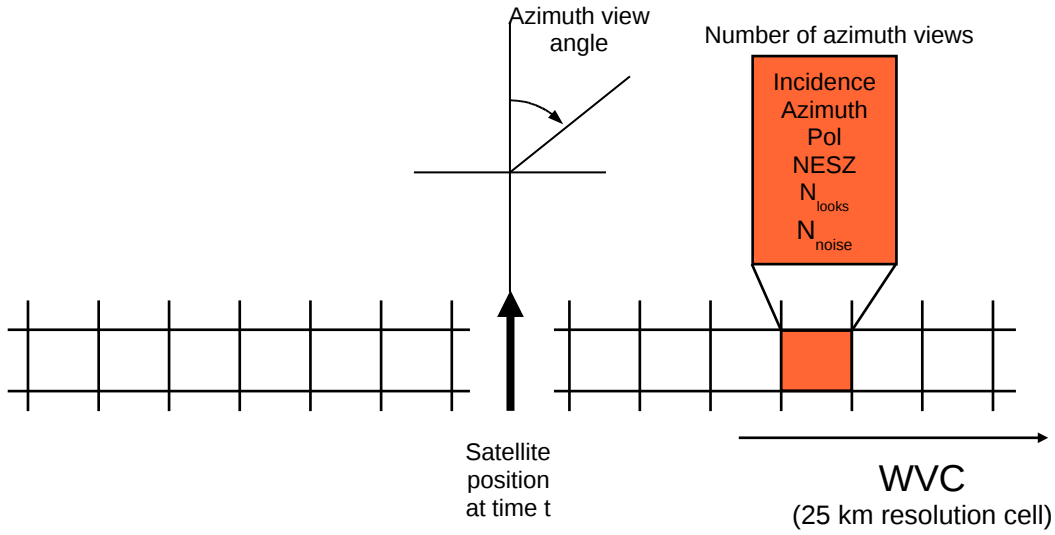

Fig. 10: Pseudo-Level 1b product on a gridded swath

Other relevant information stored in Pseudo-Level 1b files are the transmitted polarization, the single look Noise-Equivalent-Sigma-Zero (NESZ = σ^0/SNR, also known as sensitivity), and the number of independent signal and noise looks (N_{looks}, N_{noise}) available per view. The NESZ describes the σ^0 level measured when the SNR is unity.

Measurement noise:

The system noise comprises both instrumental and geophysical components. The instrumental

noise sets the system radiometric resolution and it is modeled following [9] as:

$$k_p^2 = \frac{\mathrm{var}\{\sigma^0\}}{\left(\sigma^0\right)^2} = \frac{1}{N_{looks}} + \frac{1}{SNR} + \frac{1}{N_{noise} SNR^2} \qquad (2)$$

where N_{looks} and N_{noise} refer to the number of independent signal and noise looks averaged per view, and SNR refers to the average Signal to Noise Ratio for a single look (= σ^0/NESZ).

The geophysical noise model is empirically adjusted to observed ASCAT and QuikSCAT <MLE> tables at 50 km resolution (see Appendix B) and modeled as a function of wind speed as:

$$\textit{C-band} \qquad k_{geo}(v) = 0.12 \exp(-v/12) \qquad (3)$$

$$\textit{Ku-band} \qquad k_{geo}(v) = 0.05 + 2.2 \cdot 10^{-v/2} \qquad (4)$$

The instrumental and geophysical noise contributions are assumed Gaussian and uncorrelated. For simulated observations, the total backscatter coefficient is modeled as

$$\sigma^0 = \sigma^0_{GMF}\left(1 + \sqrt{k_p^2 + k_g^2}\ N[0;1]\right) \qquad (5)$$

where N[0,1] is a Gaussian PDF with zero mean and unit standard deviation.

Fig. 11 displays typical levels of instrumental and geophysical noise observed by the QuikSCAT and ASCAT scatterometers. ASCAT backscatter noise levels are consistent with the current 3-to-10 % Kp requirement for the nominal mode (50 km resolution or 25 km gridding) at min/max backscatter conditions (i.e. low cross-wind in outer swath and high up-wind in inner swath).

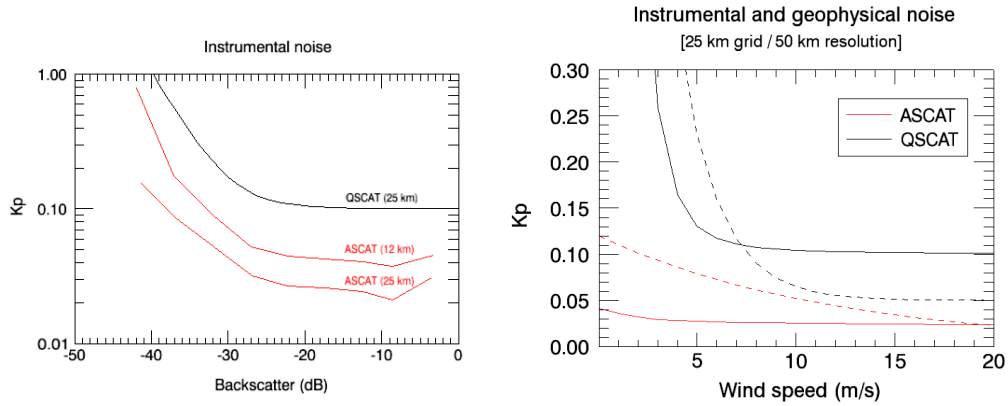

Fig. 11: Representative instrumental (continuous) and geophysical (dashed) noise levels at C and Ku-band (instrumental noise as reported in KNMI/NOAA BUFR products)

Wind retrieval:

The retrieval of ocean winds from scatterometer data relies on the use of the Geophysical Model Functions (GMFs), which relate the state variables wind speed and wind direction to backscatter measurements. The wind inversion is based on a search for minimum distances between backscatter measurements and backscatter model solutions lying on the empirical GMF surface. We define the normalized square distance MLE($\mathbf{v}|\sigma^0$) from backscatter observations σ^0 to backscatter wind solutions $\sigma^0_{GMF}(\mathbf{v})$ on the GMF surface as:

$$MLE(\vec{v} \mid \sigma^0) = \frac{1}{\langle MLE \rangle} \sum_{i=1\ldots N} \frac{\left|\sigma_i^0 - \sigma_{GMF,i}^0(\vec{v})\right|^2}{\mathrm{var}\{\sigma_i^0\}} \qquad (6)$$

where N is the dimension of the backscatter vector (i.e. the number of views per WVC node), var{σ^0} is the instrumental noise variance and <MLE> is an empirical normalization factor that accounts for deviations from the ocean wind GMF due to geophysical noise, namely sub-cell wind variability and/or rain contamination. The normalized square distance MLE is but a sum of weighted square residuals between model and observed backscatter vectors, and the wind inversion consists of a search for minimum MLE across the space of solutions. The backscatter point on the GMF surface that lies the closest to observations yields the wind output, also known as the *first rank wind solution*.

Note that the scatterometer wind retrieval performance is affected by the presence of multiple ambiguous solutions, which arise from a combination of instrumental noise, some non-ideal observation geometries and proximity between the GMF up- and downwind branches. The process of selecting a wind solution among a set of likely candidates is called ambiguity removal, and the method used at KNMI (see e.g. [12]) draws from Numerical Weather Prediction (NWP) model information for this purpose. The problem is solved by minimizing a total cost function that combines both observational and NWP background contributions as:

$$J = -2\ln(probability) = J_{obs} + J_{NWP} = -2\ln\left(P_{obs}(v \mid v_0) \cdot P_{NWP}(v - v_{NWP})\right) \qquad (7)$$

Which in terms of probabilities is equivalent to the product of the simulator output wind statistics $P_{obs}(\mathbf{v}|\mathbf{v}_0)$ times a Gaussian probability distribution $P_{NWP}(\mathbf{v}\text{-}\mathbf{v}_{NWP})$ centered about a NWP "true" wind forecast with a variance $\sigma_{NWP}^2 \sim 5$ m^2/s^2 in the wind components, resulting in an ambiguity-free output wind distribution function $P_{obs}(\mathbf{v}|\mathbf{v}_0)P_{NWP}(\mathbf{v}\text{-}\mathbf{v}_{NWP})$. Fig. 12 illustrates this ambiguity removal process. The NWP forecast variance σ_{NWP} has been chosen to be commensurate with the sum of the NWP model analysis and representativeness errors.

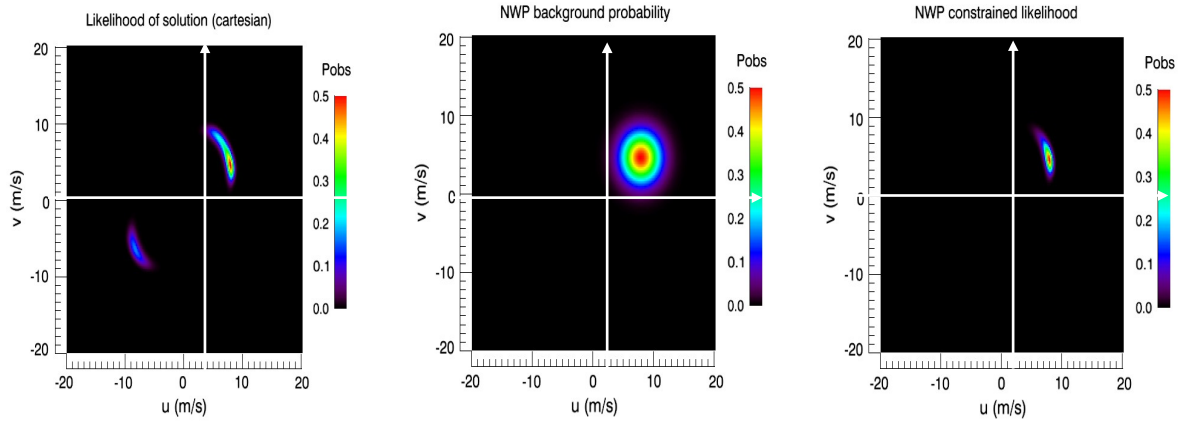

Fig. 12: Ambiguity removal in the end-to-end scatterometer performance model: Output wind statistics (left); NWP probability (center); ambiguity-free output wind statistics (right) for QuikSCAT outer swath (WVC 26) with input wind 9 m/s @ 30° and k_p = 10 % with <MLE>=5

Figure of Merit (1): Wind vector RMS error

At NWP centers, the quality of a wind measurement is usually referred to a vector RMS error.

Along this line, our first Figure of Merit (FoM) is defined as the wind vector RMS error calculated from the ambiguity-free output wind distribution and normalized by the NWP background uncertainty as:

$$FoM_{VRMS} = \frac{RMS_{obs}}{RMS_{NWP}} \in [0,1] \tag{8}$$

where

$$\begin{aligned} RMS_{obs} &= \left(\int \left| \vec{v} - \vec{v}_{true} \right|^2 P_{obs}(\vec{v} \mid \vec{v}_{true}) P_{NWP}(\vec{v} - \vec{v}_{true}) d^2 v \right)^{1/2} \\ RMS_{NWP} &= \left(\int \left| \vec{v} - \vec{v}_{true} \right|^2 P_{NWP}(\vec{v} - \vec{v}_{true}) d^2 v \right)^{1/2} = \sqrt{2}\sigma_{NWP} \end{aligned} \tag{9}$$

and $\sigma_{NWP} = \sqrt{5}$ m/s is the NWP background uncertainty standard deviation, and

$$P_{obs}(\vec{v} \mid \vec{v}_{true}) = C\chi_2^2[MLE(\vec{v} \mid \vec{v}_{true})] \tag{10}$$

$$P_{NWP}(\vec{v} - \vec{v}_{true}) = \frac{1}{2\pi\sigma_{NWP}^2} \exp\left(\left| \vec{v} - \vec{v}_{true} \right|^2 / (2\sigma_{NWP}^2) \right) \tag{11}$$

The constant *C* in Eq. (10) guarantees that the integral area under P_{obs}*P_{NWP} is unity. This FoM quantifies the standard deviation of output wind solutions about the true wind after NWP-based ambiguity removal and it should be as low as possible.

Figure of Merit (2): Ambiguity susceptibility

Another performance figure should quantify the ability of a scatterometer to handle ambiguous solutions or function without a priori NWP model information. Our next FoM is defined as the fraction of solutions that fall outside the NWP background constraint (a Gaussian distribution with a variance of 5 m^2/s^2 about the true wind) relative to the number of solutions that fall within it (see Fig. 13), expressed as:

$$FoM_{AMBI} = P_{NWP,\max} \int P_{obs}(\vec{v} \mid \vec{v}_{true}) d^2 v - 1 \quad [0, \ ] \tag{12}$$

This FoM quantifies the significance of the NWP background information for scatterometer wind retrieval (i.e. ambiguity removal) and it should be as low as possible.

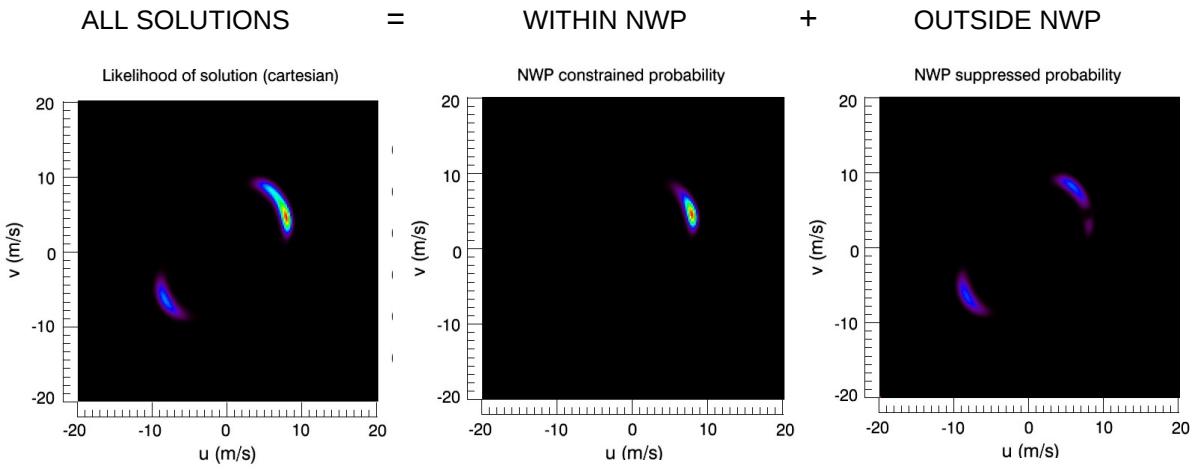

Fig. 13: Output wind statistics $P_{obs}(\mathbf{v}|\mathbf{v}_0)$ (left); ambiguity-free solutions $P_{obs}(\mathbf{v}|\mathbf{v}_0)P_{NWP}(\mathbf{v}\text{-}\mathbf{v}_{NWP})$ (center); NWP suppressed solutions $P_{obs}(\mathbf{v}|\mathbf{v}_0)(P_{NWP,max} - P_{NWP}(\mathbf{v}\text{-}\mathbf{v}_{NWP})$ (right), for

QuikSCAT outer swath (WVC 26) with input wind 9 m/s @ 30° and k_p = 10 % with <MLE>=5

Figure of Merit (3): Bias errors

Bias errors arise from degrees of asymmetry (or skewness) in the output wind statistics functions, which cause the mean of the distribution (or average location of the output wind solution) to be shifted from the distribution mode (or location of the true wind, see Figure 11). Systematic wind biases can be calculated along the wind radial and azimuth directions as:

$$bias_{spd} = v_{true} - \int v \, P_{obs}(\vec{v} \mid \vec{v}_{true}) P_{NWP}(\vec{v} - \vec{v}_{true})\big|_{\phi=\phi_{true}} \, dv \qquad (13)$$

$$bias_{dir} = \phi_{true} - \int \phi \, P_{obs}(\vec{v} \mid \vec{v}_{true}) P_{NWP}(\vec{v} - \vec{v}_{true})\big|_{|v|=|v_{true}|} \, d\phi \qquad (14)$$

Because systematic errors along the wind radial direction (output windspeed biases) are small in general, we will not consider them further in this report. However, the presence of systematic errors along the wind azimuth direction (output wind direction biases) produces artificial directional preferences that may corrupt the observed wind climatologies (see, e.g. QuikSCAT case in Section 4.1).

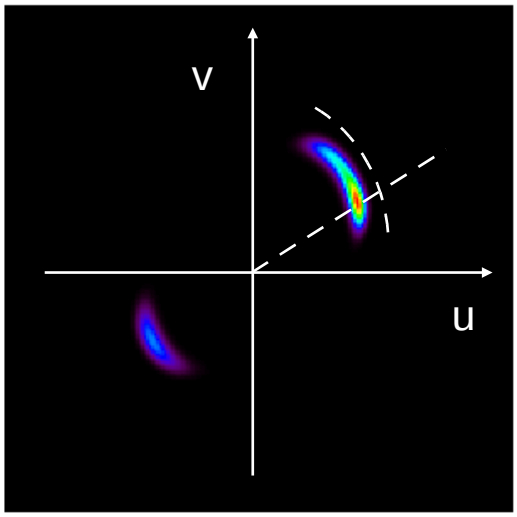

Fig. 14: Skewed output wind statistics give way to systematic biases in wind speed and most notably, in wind direction. In this example, the true wind lies at 9 m/s @ 30 degrees but the wind outputs seem drawn to a 45 degrees solution (QuikSCAT, WVC = 26)

6. Wind Retrieval Performance

Figs. 15 and 16 summarize the performance figures for the fixed fan-beam and rotating fan-beam concepts using instrumental noise levels that comply with the technical requirements and geophysical noise levels as defined by Eq. (3). For the latter concept, three different rotation rates have been considered in this performance estimation (1, 2 and 3 RPM). Fig. 15 shows the three FoMs as function of across-track nodal position and wind direction for 9 m/s wind. It is re-called that the results are normalised to the NWP background uncertainty of $\sqrt{10}$ m/s. The upper pictures give results for the fixed fan-beam concept and the lower pictures for the rotating fan-beam concept with 2 RPM antenna scan speed. Fig. 16 shows a more condensed result as a function of the across-track position only. Here, the FoMs have been averaged over all wind directions and wind climatology.

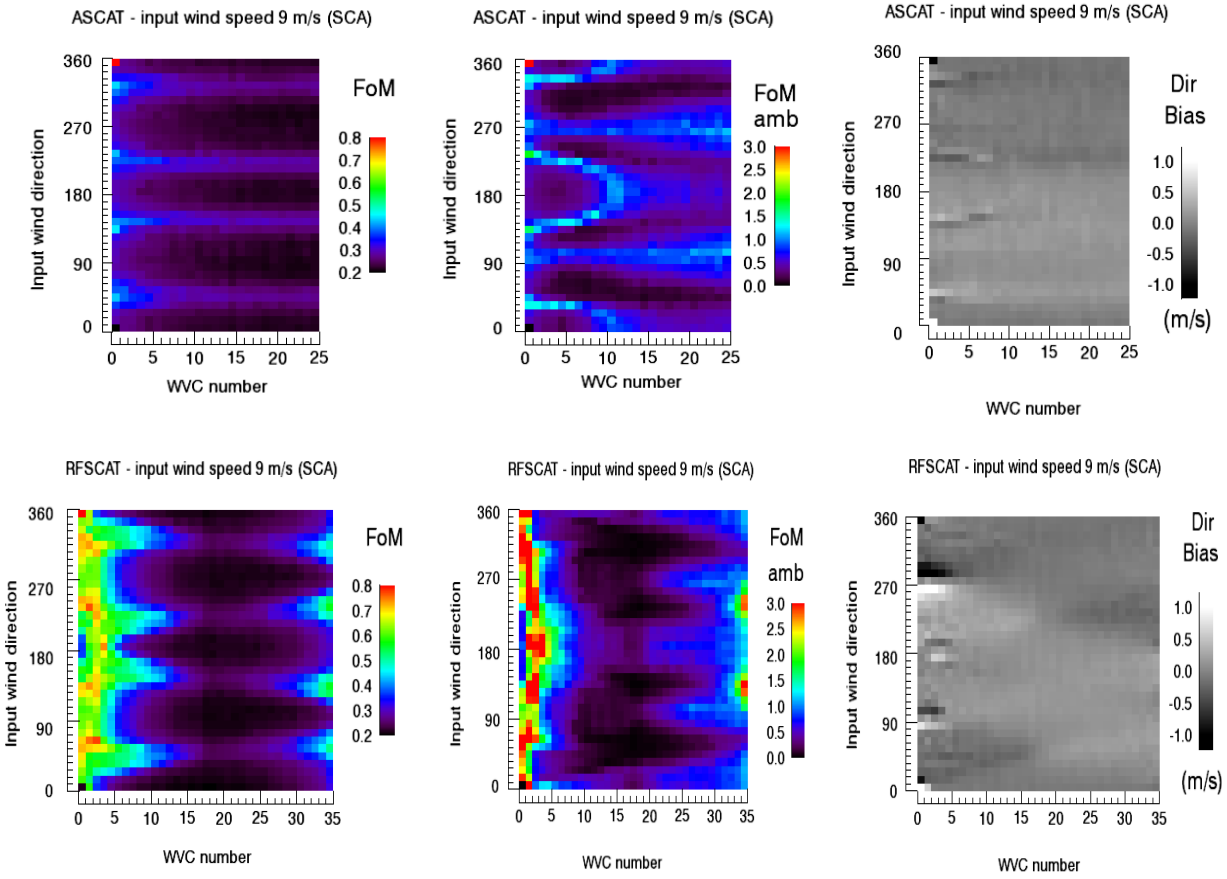

Fig. 15: Fixed fan-beam (top row) and totating fan-beam (2 RPM, bottom row) FoMs as a function of across-track location and wind direction (wind speed is 9 m/s)

FoM scores indicate that the wind quality of the fixed fan-beam concept remains quite uniform across the swath (Fig. 15 – upper). There is a slight performance degradation at a number of distinct zones in wind direction, which reflects the particular measurement geometry of this concept and properties of the GMF. The retrieval performance also slightly decreases towards the low incidence end of the swath, which was actually expected due to the relaxation of the radiometric resolution requirement below 25° incidence. As a matter of fact, this relaxation was introduced in order to limit the radar power at a reasonable level.

The performance of the rotating fan-beam concept (Fig. 15 – lower) depends strongly on across-track location and degrades significantly at nadir and the swath edges as anticipated. Similar to the case of the fixed fan-beam concept, there is also a slight performance modulation as a function of the wind direction. The performance of this concept depends strongly on the antenna rotation speed as seen in Fig. 16 (red curves). In any case, the extent of the comparably useful swath remains similar for both the fixed and rotating fan-beam concepts and is limited to about 650 km (single side) for a wind vector RMS error of ≤ 0.6 m/s if the antenna scan rate of the latter is ≥ 2 RPM. Retrieved wind from regions outside the useful swath will not be used for numerical weather predictions. A definite strength of the rotating fan-beam concept lies in its very low ambiguity scores (low dependability on NWP background support for ambiguity removal) over the extent of its usable swath. The larger azimuth diversity of the measurements seems to contribute to this trend. Another attractive feature of this concept is the smaller nadir-gap (approx. 200 km), as compared to the fixed fan-beam concept, for obtaining better synoptic view of large-scale storm events and better

synergy with other companion payloads with observations centered on nadir.

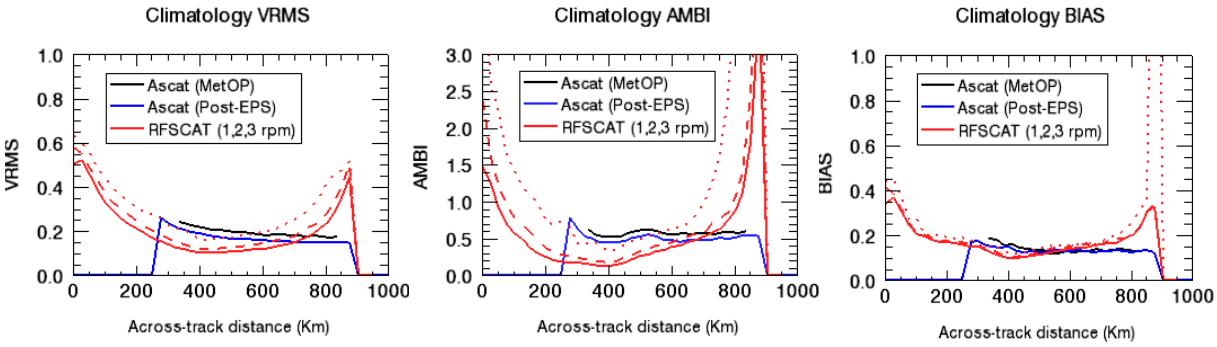

Fig. 16: Average climatology FoMs for fixed fan-beam concept (blue) and rotating fan-beam concept (red) as a function of across-track distance. ASCAT performance on *MetOp* is shown in black for reference

To gain an appreciation on how geophysical noise affects the SCA performance figures, Fig. 17 shows the FoMs with and without geophysical noise. Observe that the geophysical noise contribution accounts for about a half of the simulated wind vector RMS error (left most picture), whereas the ambiguity susceptibility increases significantly (central picture). The impact of geophysical noise on wind bias appears to be low, as the former is uniform over all wind direction.

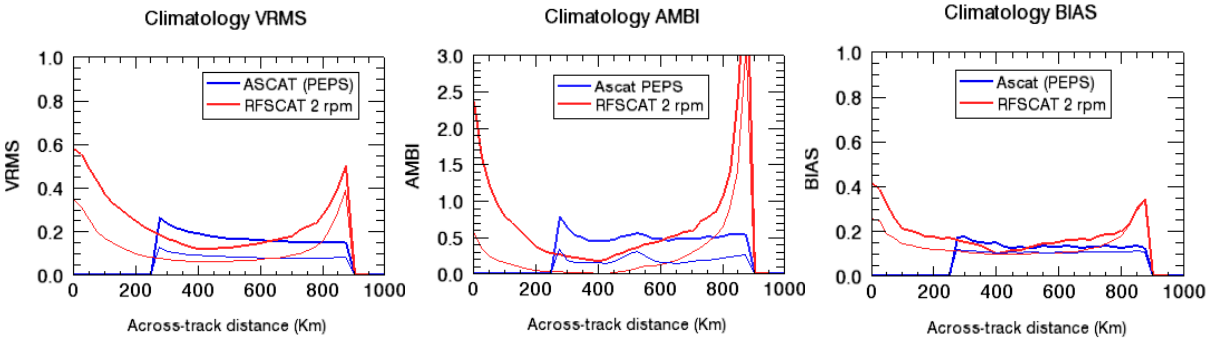

Fig. 17: Average climatology FoMs for fixed fan-beam concept (blue) and rotating fan-beam concept (2 rpm, red) as a function of across-track distance with (thick line) and without (thin line) geophysical noise

Finally, Fig. 18 shows the performance of the selected baseline (fixed fan-beam) concept for wind speed below 8 m/s. Such analysis is of relevance when one wishes to compare the scatterometry against the passive microwave polarimetry (e.g. WindSat [13]) as the latter is known to have degraded retrieval performance in wind direction at lower wind speed. It is seen that the vector RMS error remains below 1.3 m/s for 3 m/s wind.

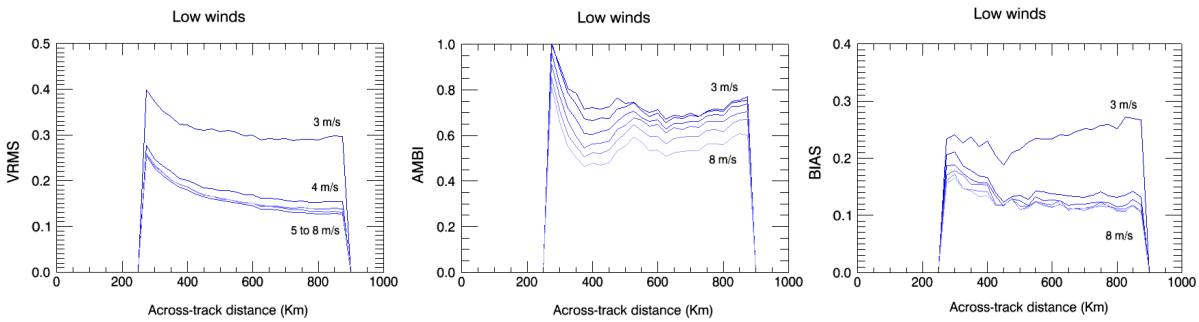

Fig. 18: Low wind FoMs (≤ 8 m/s) for the fixed fan-beam (baseline) concept as a function of across-track distance.

7. Conclusion

A fixed fan-beam scatterometer concept, similar to the *MetOp*'s ASCAT instrument, has been selected for the Post-EPS mission at the end of Phase 0. The trade-offs during Phase 0 considered three distinct instrument concepts, out of which the fixed fan-beam and rotating fan-beam concepts were compared in more details in terms of engineering design and end-to-end wind retrieval performance. A uniform and objective methodology for the performance assessment of dissimilar scatterometer concepts has been developed. The performance model rests on statistics produced by an end-to-end scatterometer wind retrieval simulator run in a Monte Carlo fashion. Three Figures of Merit have been proposed as a means to examine the different aspects that affect the quality of scatterometer wind products: the wind vector RMS error; the susceptibility to ambiguities; and the presence of biases. The performance model results reveal and quantify the inherent capabilities of different scatterometer configurations under realistic instrumental and geophysical noise condition. The performance model results indicate that the wind retrieval performance of the fixed fan-beam concept is rather uniform across the swath, while that of rotating fan-beam concept remains strongly dependent on across-track location, degrading at nadir and the swath edges as expected due to the unfavorable measurement geometry in those parts of the swath. Nevertheless, the performance of the latter is comparable to that of the former in terms of FoMs and usable swath extensions. Therefore, both concepts can meet the observation requirements of the Post-EPS mission, with a slight strength of the rotating fan-beam concept for its higher robustness against wind directional ambiguity, allowing to rely less on the accuracy of the background wind field. Work during the upcoming Post-EPS Phase A will include further refinements in instrument design definition and corresponding performance sensitivity studies. This will also include investigation of feasibility in adding a HH-polarisation capability in conjunction with its usefulness at high wind speeds and the refinement of the scatterometer geophysical noise models.

References

[1] M. Betto**,** C. Accadia, S. Banfi P. Bensi, J-L. Bézy, V. Kangas, S. Kraft, C.C. Lin, R. Meynart, P. Phillips, L. Sarlo, P. Silvestrin, P. Schluessel, J. Wilson, "Post-EPS System Concept," EUMETSAT Meteorological Satellite Conference, 21-25 Sept 2009, Bath, UK.

[2] S. Banfi, P. Schlüssel, C. Keegan, M. Betto, C.C. Lin, V. Kangas, S. Kraft, P. Bensi, I. Zerfowski, M. Saccoccio and T. Maciaszek, "Feasibility Studies for the follow-on EUMETSAT Polar System," SPIE Remote Sensing Europe Int'l Symposium, Toulouse,

France, Sept. 2010.

[3] C.C. Lin, J. Wilson, F. Impagnatiello and P.S. Park, “An Analysis of a Rotating, Range-Gated, Fanbeam Spaceborne Scatterometer Concept,” IEEE Trans. Geosc. & Remote Sensing, Vol. 38, Sept. 2000, pp2114-2121.

[4] A. Verhoef, M. Portabella, A. Stoffelen and H. Hersbach, CMOD5.n - the CMOD5 GMF for neutral winds, OSI SAF report, SAF/OSI/CDOP/KNMI/TEC/TN/165, 2008, available at http://www.knmi.nl/scatterometer/publications/

[5] M. Portabella and A. Stoffelen, “Scatterometer Backscatter Uncertainty due to Wind Variability,” IEEE Trans. Geosc. & Remote Sensing, Vol. 44, Nov. 2006, pp3356-3362.

[6] M.W. Spencer, C. Wu and D.G. Long, “Improved resolution backscatter measurements with the SeaWinds Pencil-Beam Scatterometer,” IEEE Trans. Geosc. & Remote Sensing, Vol. 38, Jan. 2000.

[7] C.C. Lin, J. Wilson, F. Impagnatiello and P.S. Park, “Rotating, Range-Gated Fanbeam Imaging Radar: A New Spaceborne Scatterometer Concept,” PIERS Workshop on Advances in Radar Methods, Baveno, July 1998.

[8] C.C. Lin, A. Stoffelen, J. de Kloe, V. Wismann, S. Bartha, H.-R. Schulte, “Wind Retrieval Capability of Rotating, Range-Gated, Fanbeam Spaceborne Scatterometer,” SPIE Int’l Symposium on Remote Sensing, 23-27 Sept. 2002, Crete, Greece.

[9] R.E. Fischer, “Standard Deviation of Scatterometer Measurements from Space,” IEEE Trans. on Geoscience Electronics, Vol. GE-10, No. 2, April 1972, pp. 106-113.

[10] Liu, W. T., W. Tang, and X. Xie, “Wind power distribution over the ocean,” Geophys.

Res. Lett., 35, L13808, doi:10.1029/2008GL034172, 2008.

[11] F. J., Wentz, and D. K. Smith, “A Model Function for the Ocean-Normalized Radar Cross Section at 14 GHz Derived From NSCAT Observations,” J. Geophys. Res., 104(C5), 11499-11514, 1999.

[12] J. Vogelzang, “Two dimensional variational ambiguity removal (2DVAR)”, Technical Report NWPSAF-KN-TR-004, EUMETSAT, 2007.

[13] WindSat Home Page: http://www.nrl.navy.mil/WindSat/